American Mineralogist, Volume 70, pages 317–331, 1985

Redox equilibria and the structural states of ferric and ferrous iron in melts in the system $CaO–MgO–Al_2O_3–SiO_2–Fe–O$: relationships between redox equilibria, melt structure and liquidus phase equilibria

BJØRN O. MYSEN, DAVID VIRGO, ELSE-RAGNHILD NEUMANN,[1] AND FRIEDRICH A. SEIFERT[2]

Geophysical Laboratory, Carnegie Institution of Washington
Washington, D.C. 20008

Abstract

Relationships between melt structure and redox equilibria of iron in $CaO–Al_2O_3–SiO_2–Fe–O$ and $MgO–Al_2O_3–SiO_2–Fe–O$ melts with Ca/Al and Mg/Al $\geqq 0.5$ have been determined with Mössbauer spectroscopy at 1 atm pressure. These data and published phase equilibria in iron-free systems were used to calculate liquidus equilibria involving iron-bearing melts and iron-free minerals.

Ferrous iron is a network modifier (probably in octahedral coordination) in all compositions studied. Ferric iron is tetrahedrally coordinated in melts with $Fe^{3+}/\Sigma Fe > 0.5$, and undergoes a gradual coordination transformation in the $Fe^{3+}/\Sigma Fe$ range between 0.5 and 0.3. In this $Fe^{3+}/\Sigma Fe$-range, tetrahedrally- and octahedrally-coordinated ferric iron may coexist. The temperature-dependence of the Mössbauer hyperfine parameters and the temperature-independence of the intensity of the absorption envelope are consistent with a local structural unit that may be stoichiometrically similar to Fe_3O_4. The Fe^{2+}/Fe^{3+} is linearly correlated with polymerization (nonbridging oxygens per tetrahedrally coordinated cations, NBO/T) and Al/(Al + Si) of the melt. There are linear relationships between log (Fe^{2+}/Fe^{3+}) and log f_{O_2} and between log (Fe^{2+}/Fe^{3+}) and $1/T$ (absolute temperature). The standard-state free energy of reduction of ferric to ferrous iron, calculated from these lines, decreases with increasing Z/r^2 (ionization potential) of the alkaline earth metal cation, with decreasing bulk melt NBO/T (more polymerized melts) and with decreasing Al/(Al + Si) of the melt.

In magnesium aluminosilicate melts with NBO/T = 0.6 and Al/(Al + Si) = 0.2 (typical values for quartz tholeiite and basaltic andesite) with 10 wt.% iron oxide added as Fe_2O_3 the liquidus phase is tridymite when equilibrated with air. Calculations indicate that at f_{O_2} between 10^{-2} and 10^{-3} atm the liquidus phase changes to protoenstatite, and then to forsterite at even lower oxygen fugacities. Substitution of Ca (or Na) for Mg results in expansion of the metasilicate (pyroxene) liquidus field and contraction of that of tridymite. Fractional crystallization trends of magmatic liquids are, therefore, significantly dependent on oxygen fugacity, degree of polymerization of the magma (NBO/T), Al/(Al + Si) and the relative abundance of alkali metals and alkaline earths.

Introduction

Crystal–liquid equilibria of natural magmatic liquids depend on the structures of both the melt and the minerals. The liquidus phase equilibria in the systems $CaO–Al_2O_3–SiO_2$ (Osborn and Muan, 1960a) and $CaO–Fe_2O_3–SiO_2$ (Osborn and Muan, 1960b) indicate that the influence of Fe^{3+} and Al^{3+} on the phase relations at 1 atm pressure are similar (Fig. 1). These available data suggest that the influence of Al^{3+} and Fe^{3+} on the anionic structure of the melts in these two ternary systems may resemble each other. With the same degree of polymerization of the melts (recalculated as nonbridging oxygens per tetrahedrally coordinated cations, NBO/T[3]), re-

[1] Present address: Mineralogisk-Geologisk Museum, University of Oslo, Sars gt. 1, Oslo 5, Norway.

[2] Present address: Mineralogisch-Petrographisches Institut, Universitat Kiel, Olshaussenstr. 40-60, 2300 Kiel, Federal Republic of Germany.

[3] The use of NBO/T as a compositional indicator requires melt structural information. The NBO/T can be calculated from chemical compositions as shown by Mysen et al. (1982a, 1984a) after assignment of tetrahedrally-coordinated cations. As shown elsewhere (for review of information, see Mysen et al., 1982a, 1984b; McMillan and Piriou, 1983), Al^{3+}, Ti^{4+} and P^{5+} most likely are tetrahedrally-coordinated in silicate melts compositionally relevant to magmatic processes. The structural role of Fe^{3+} is more complex, and is the subject of the present report. The NBO/T, when calculated from bulk compositions in this paper, includes ferric iron only after its structural position in a given melt has been specifically discussed. As summarized by Mysen et al. (1982a), free oxygen (that is oxygen that is not bonded to any tetrahedrally-coordinated cation) is not likely in silicate melts as polymerized as natural magmatic liquids. With this information, the NBO/T can be used as an expression of overall degree of polymerization of silicate melts as well as a structural indicator of individual anionic units in the melts.

0003–004X/85/0304–0317$02.00

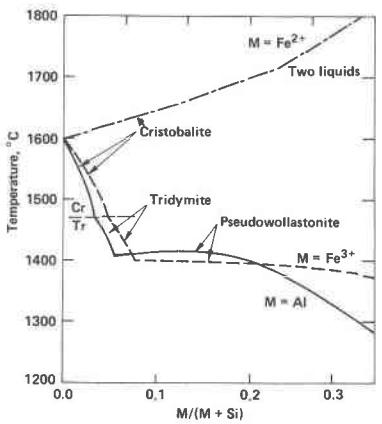

Fig. 1. Liquidus phase equilibria in the systems $CaO–Al_2O_3–SiO_2$, $CaO–Fe_2O_3–SiO_2$ and $CaO–FeO–SiO_2$ as a function of Al/(Al + Si), $Fe^{3+}/(Fe^{3+} + Si)$ and $Fe^{2+}/(Fe^{2+} + Si)$ for melts with bulk NOB/T = 1. (Data from Osborn and Muan, 1960a,b,c.)

placement of Si^{4+} by Al^{3+} or Fe^{3+} leads to a rapid reduction of the silica-polymorph liquidus temperature and a transition from tridymite to pseudowollastonite on the liquidus at approximately the same temperature and the same $M^{3+}/(M^{3+} + Si^{4+})$ ($M^{3+} = Al^{3+}$ or Fe^{3+}) (Fig. 1). These trends indicate that the activity of the SiO_2 component decreases and that of the metasilicate increases at nearly the same rate as the $M^{3+}/(M^{3+} + Si^{4+})$ increases both for $M^{3+} = Al^{3+}$ and Fe^{3+}. Aluminum is in tetrahedral coordination provided that there is sufficient alkali or alkaline earths for charge-balance of Al^{3+} in the melts (Taylor and Brown, 1979a,b; Hess and Wood, 1982; Seifert et al., 1982). Ferric iron may also be in tetrahedral coordination at least in iron-bearing melts equilibrated with air (see also Mysen and Virgo, 1978; Brown et al., 1978; Dickenson and Hess, 1981; Calas and Petiau, 1983). These liquidus phase equilibria in the systems $CaO–Al_2O_3–SiO_2$ and $CaO–Fe_2O_3–SiO_2$ differ dramatically, however, from those with all iron as Fe^{2+} (Fig. 1; see also Osborn and Muan, 1960c), where replacement of Si^{4+} by Fe^{2+} (and a concomitant decrease in Ca^{2+} to maintain a constant NBO/T) results in an increase in the temperature of the cristobalite liquidus and the appearance of two liquids as the composition approaches the join $FeO–SiO_2$. It is suggested, therefore, that both ferric and ferrous iron have an important influence on the melt structure but that the effect of the two cations is quite different.

In addition to the seemingly important impact of iron oxides on the structure of silicate melts relevant to magmatic liquids (and, thus, properties that are affected by melt structure), redox equilibria of iron are also of intrinsic interest because such data may be used to deduce temperature–oxygen fugacity histories of magma (e.g., Haggerty, 1978; Haggerty and Tompkins, 1983; Sato and Valenza, 1980). It is necessary, therefore, to calibrate $Fe^{3+}/\Sigma Fe$ as a function of intensive and extensive variables (see, e.g., Sack et al., 1980; Thornber et al., 1980; Kilinc et al., 1983, for empirical calibration of redox ratios of magmatic liquids). The physicochemical principles that govern the redox equilibria must be established before such data will have general applicability to natural magmatic processes.

The present study was conceived to address some of the principal features of redox equilibria of iron oxides that are interrelated with the structure of silicate melts and equilibria between melts and minerals. In this report, relationships between Al/(Al + Si), NBO/T, types of charge-balancing metal cations and oxygen fugacity have been evaluated. Inasmuch as peraluminous magmatic liquids are comparatively rare, the compositions of the melts were chosen so that $(Al + Fe^{3+})$ is always less than the sum of alkaline earth metal cations.

Experimental methods

Starting materials in the systems $CaO–Al_2O_3–SiO_2–Fe_2O_3$ and $MgO–Al_2O_3–SiO_2–Fe_2O_3$ were prepared from spectroscopically pure SiO_2, Al_2O_3, Fe_2O_3, MgO and $CaCO_3$ in batches of 200 mg and ground under alcohol for 1 hr before use. The Fe_2O_3 was isotopically enriched with ^{57}Fe to about $^{57}Fe/\Sigma Fe = 0.1$ to facilitate Mössbauer spectroscopic analysis. The aluminosilicate compositions are denoted MAS and CAS for the MgO- and CaO-bearing systems, respectively. The weight percentage of Fe_2O_3 added to the starting marterials is indicated by the symbols F5 and F10 (5 and 10 wt.% Fe_2O_3, respectively). Roman numerals (I to XIII) refer to iron-free compositions where NBO/T and Al/(Al + Si) are similar (Fig. 2). In each system there is a series with variable Al/(Al + Si) (0.14–0.43) and constant NBO/T (0.67) and a series with constant Al/(Al + Si) (0.334) and changing NBO/T (0.17–1.33). In the system CAS, there is an additional composition line with different but constant NBO/T (0.86) and changing Al/(Al + Si) (0.05–0.43). Finally, there is a composition line that covers a range of compositions where both Al/(Al + Si) and NBO/T are variable (in the ranges 0.08–0.43 and 0.16–0.86, respectively). These compositional ranges were chosen to cover those commonly observed in natural magmatic liquids.

Sintered 20–25 mg pellets of the oxide starting materials were suspended on single loops of 0.004-in.-diameter Pt wire with the weight ratio of the sample to Pt about 100. These pellets were transformed to a melt in $MoSi_2$-heated, vertical quench furnaces. The samples were quenched in water at a quenching rate exceeding 500°C/sec. The oxygen fugacity was controlled with $CO–CO_2$ gas mixtures where the f_{O_2} was monitored with a Y_2O_3-doped ZrO_2 oxygen sensor (Sato, 1972), supplied by Oxide Fabricators, Inc., Victoria, Australia. The oxygen fugacity, as calibrated against nickel–nickel oxide and iron–wustite oxide buffers (Chou, 1978) and calculated CO/CO_2 (Deines et al., 1974), is accurate to within 0.05 log unit. Precision is better than 0.02 log unit. The temperatures were monitored with one thermocouple 1 cm above the sample and one within the oxygen sensor (displaced 1 cm horizontally from the sample). The temperatures, as checked against the melting point of Au (1062.5°C), are accurate to within ±5°C and precise to ±1°C.

Electron microprobe analyses show that the compositions of the run products are in accord with nominal compositions within analytical uncertainty (approximately 2%, relative) except for iron. As much as a 5% iron-loss to the Pt wire-loop (relative to the total amount added) was encountered in experimental charges under the most reducing f_{O_2} conditions. Electron microprobe

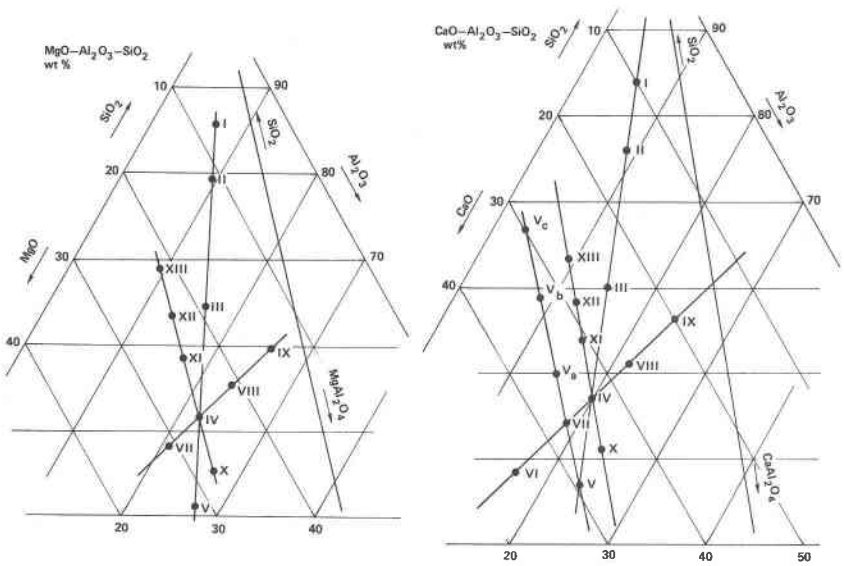

Fig. 2. Composition of iron-free end-member starting materials in the systems $MgO–Al_2O_3–SiO_2$ and $CaO–Al_2O_3–SiO_2$. See text for additional discussion of bulk compositional relationships.

analyses of the run products are available from the authors upon request.

The redox ratio of iron and structural information on Fe^{2+} and Fe^{3+} in the quenched samples were obtained with ^{57}Fe resonant absorption Mössbauer spectroscopy. The spectra are fitted with least-squares minimization (Davidon, 1959) to one ferric doublet and one or two ferrous doublets. Several alternative fitting methods, using quenched melts in the systems $Na_2O–SiO_2–Fe–O$, $BaO–SiO_2–Fe–O$, $CaO–SiO_2–Fe–O$, $MgO–SiO_2–Fe–O$, $Na_2O–Al_2O_3–SiO_2–Fe–O$, $CaO–Al_2O_3–SiO_2–Fe–O$ and $MgO–Al_2O_3–SiO_2$ have been evaluated and will be discussed in detail in a separate paper (Virgo and Mysen, 1985). Only a brief summary of the principles and the most important conclusions will, therefore, be presented here.

These fitting routines include those in which it is assumed that the cumulative envelope of the absorption spectra consists of a number of overlapping elementary doublets of Lorentzian shape, and those in which it is assumed that the hyperfine parameters (isomer shift and quadrupole splitting) are linearly correlated (Wivel and Morup, 1981; Danckwerth and Virgo, 1982; Danckwerth et al., 1982; Virgo and Mysen, 1985). Another method, in which a variable number of doublets, of pure Lorentzian line shape, are assumed for either Fe^{2+} or Fe^{3+}, has been predominantly used in the present analysis of the spectra. This method of deconvolution results in fits that on statistical grounds are comparable to those obtained by fitting hyperfine parameter distributions. As discussed in more detail elsewhere (Virgo and Mysen, 1985), the velocities of the component peaks of the quadrupole split doublets of Fe^{3+} and Fe^{2+} and the $Fe^{3+}/\Sigma Fe$ derived with the two fitting methods are within 5% (relative) of each other. Furthermore, in choosing between, for example, single or multiple Fe^{3+} and Fe^{2+} doublets when fitting separate doublets of Lorentzian line shape (Virgo and Mysen, 1985, see also Mysen et al., 1984), the average values of the hyperfine parameters (isomer shift and quadrupole splitting) in the simplest two-doublet (one ferric and one ferrous) fits are within 5% of the weighted averages from fits of multiple doublets.

It may be argued that the Mössbauer spectra of silicate glasses theoretically are best described in terms of a distribution of the hyperfine field. The simpler fitting routine, using a limited number of ferrous and ferric doublets of Lorentzian line shape was, however, employed. This decision was made partly because of the excessive CPU time required for the least-squares fitting of the hyperfine parameters, and partly (and for the present purpose more important) because the structural information discussed in the present paper and the $Fe^{3+}/\Sigma Fe$ obtained from these fits are consistent with those obtained with the more complex fits of the spectra (Danckwerth et al., 1982; Virgo and Mysen, 1985) and also with independently obtained information.

It is proposed here that the melt structural correlations with doublets of pure Lorentzian shape are also compatible with a more realistic model of melt structure in which information from Raman (Brawer, 1975; Furukawa et al., 1981; Mysen et al., 1980a,b, 1982a), infrared (Domine and Piriou, 1983), transmission electron microscopy (Gaskell, 1975) and ^{29}Si NMR spectroscopic techniques (Kirkpatrick et al., 1982) indicate the existence of distinct (20–100Å) chemical and structural units in silicate melt structures.

In using this fitting method, all doublets were constrained to have equal areas. For ferric iron, the halfwidths were also constrained to be equal. The cumulative envelope of highly reduced glasses (no Fe^{3+} present) is, however, typically asymmetric (e.g., Mao et al., 1973; Mysen and Virgo, 1978; Levitz et al., 1980). Thus, in the fitting procedure, the half-widths were not constrained for the Fe^{2+} doublets.

The $Fe^{3+}/\Sigma Fe$ [or $Fe^{2+}/Fe^{3+} = (1 - Fe^{3+}/\Sigma Fe)/(Fe^{3+}/\Sigma Fe)$] is obtained from relative areas of doublets. The redox ratio thus obtained is within 7% (relative) of the results from wet chemical analysis (Table 1). With an approximately 3–5% relative uncertainty in the Mössbauer data (as indicated by replicate analyses, replicate experiments and measurements at two different absorber temperatures, 77 and 298 K) and a 6% uncertainty reported (Sack et al., 1980) for the wet chemical method, it is considered that a 7% difference is within the cumulative analytical uncertainty of

Table 1. Comparison of $Fe^{3+}/\Sigma Fe$ determined by wet-chemical and Mössbauer spectroscopic methods

Sample	Wet chemistry	Mössbauer spectroscopy
001*	0.80 ± 0.05	0.86 ± 0.04
002*	0.88 ± 0.05	0.96 ± 0.05
004*	0.60 ± 0.04	0.65 ± 0.03
010*	0.89 ± 0.05	0.96 ± 0.05
FeAb*	0.75 ± 0.05	0.82 ± 0.04
MV78†	0.68 ± 0.04	0.71 ± 0.04

*Sample provided by Dr. I. S. E. Carmichael, University of California, Berkeley. Redox data are from Mo et al. (1982) and Carmichael (personal communication, 1983). Uncertainty in these wet-chemical analyses is 6%. For bulk chemical analyses of these samples, see Table 1 of Mo et al. (1982).

†From Mysen and Virgo (1978). Bulk composition (by weight): $An_{46}Fo_{16.2}(SiO_2)_{29.7}(Fe_2O_3)_{8.1}$ (Osborn, personal communication, 1977; as quoted by Mysen and Virgo, 1978).

the two methods (wet chemistry and Mössbauer resonant absorption).

Results

Oxygen coordination around ferric and ferrous iron

Representative ^{57}Fe Mössbauer spectra are shown in Figure 3, and a complete set of calculated $Fe^{3+}/\Sigma Fe$ and hyperfine parameters from all spectra is given in Table 2. The hyperfine parameters in Table 2 are calculated from the statistically best fits (whether with one or two ferrous doublets). Except for the most oxidized samples, the inclusion of the Fe^{2+}(II) doublet results in a 20–25% improvement in the values of χ^2, and the residual distribution becomes more random. When its inclusion was not justified statistically, the second doublet was not included.

Topologically, changes in the spectra as a function of Al/(Al + Si), NBO/T and f_{O_2} are similar in both systems. The spectra have been interpreted to consist of one ferric and generally two ferrous doublets except under the most reducing conditions ($f_{O_2} = 10^{-6} - 10^{-9}$ atm), where there is no indication of ferric iron. When either one or two ferrous doublets were statistically permissible, the velocities of the ferric iron component peaks were independent of the number of ferrous doublets.

The high-velocity component of ferric iron shifts from −0.7 mm/sec to 0.9–1.0 mm/sec as $Fe^{3+}/\Sigma Fe$ is reduced below 0.3 (Fig. 3, Table 2). The low-velocity component of the Fe^{3+} doublet is shifted from ~ -0.5 mm/sec to ~ 0 mm/sec in the same $Fe^{3+}/\Sigma Fe$ range. A transition occurs in the $Fe^{3+}/\Sigma Fe$ range between 0.5 and 0.3, within which range intermediate velocities were obtained. Within this transition range there is an increase in line width of the Fe^{3+} component peaks (from ~ 0.7 mm/sec to ~ 1.0 mm/sec). The velocity changes are reflected in an increase in the isomer shift (IS) [from ~ 0.3 mm/sec (relative to Fe metal) in the most oxidized samples to between 0.6 and 0.65 mm/sec for samples with $Fe^{3+}/\Sigma Fe < 0.3$–0.4]. The increase in $IS_{Fe^{3+}}$ is associated with a general decrease in quadrupole splitting (QS) (Fig. 4) although the $QS_{Fe^{3+}}$ trend is considerably more scattered than that of the $IS_{Fe^{3+}}$. Similar relationships between $IS_{Fe^{3+}}$, $QS_{Fe^{3+}}$ and $Fe^{3+}/\Sigma Fe$ have been observed in the analogous sodium aluminosilicate system (Virgo et al., 1983; Mysen and Virgo, 1983a; Virgo and Mysen, 1985) and in the aluminum-free Ca- and Mg-silicate systems (Mysen and Virgo, 1983b; Mysen et al., 1984). These results may indicate the existence of a second ferric iron doublet. This hypothetical doublet could not be inserted in the fits without imposed constraints on its quadrupole splitting. Without independent information on the values of the quadrupole splitting, insertion of such a doublet with the quadrupole splitting constrained was not attempted. It is noted, however, that in the analogous $Fe^{3+}/\Sigma Fe$ transition range in the system Na_2O–Al_2O_3–SiO_2–Fe–O, it has been found (Virgo and Mysen, 1985) that with those somewhat more resolved spectra, a second ferric doublet could be included. The present spectra are, however, merely consistent with such a possibility.

In the more oxidized samples ($Fe^{3+}/\Sigma Fe > 0.5$) the values of $IS_{Fe^{3+}}$ and $QS_{Fe^{3+}}$ are generally similar to those observed for tetrahedrally coordinated ferric iron in crystalline silicates (e.g., Hafner and Huckenholz, 1971; Annersten and Halenius, 1976; Mysen et al., 1980a; Amthauer et al., 1977; Waychunas and Rossman, 1983). Moreover, these values are similar to those found for iron-bearing glasses where other spectroscopic data (EXAFS, EPR, fluorescence and Raman spectroscopy) also suggest that Fe^{3+}(IV) exists (Brown et al., 1978; Calas et al., 1980; Fox et al., 1982; Virgo et al., 1981, 1982; Calas and Petiau, 1983; Mysen and Virgo, 1983b; Mysen et al., 1980a, 1984).

The gradual increase in $IS_{Fe^{3+}}$ from values near 0.3 mm/sec (298K) with $Fe^{3+}/\Sigma Fe \geqq 0.5$ to values between 0.6 and 0.7 mm/sec at $Fe^{3+}/\Sigma Fe < 0.4$ (Fig. 4) (with a concomitant decrease in $QS_{Fe^{3+}}$) may indicate a significant change in the structural position of ferric iron in these aluminosilicate melts as a function of $Fe^{3+}/\Sigma Fe$. Similar changes in hyperfine parameters for ferric iron as a function of $Fe^{3+}/\Sigma Fe$ have been observed in the systems Na_2O–SiO_2–Fe–O, CaO–SiO_2–Fe–O, MgO–SiO_2–Fe–O and Na_2O–Al_2O_3–SiO_2–Fe–O (Mysen et al., 1984a; Virgo and Mysen, 1985). Raman spectra of quenched melts in the system CaO–SiO_2–Fe–O (Mysen et al., 1984) and Na_2O–SiO_2–Fe–O (Virgo et al., 1982, 1983; Mysen and Virgo, 1983c) indicate that this increase in $IS_{Fe^{3+}}$ was associated with a systematic decrease in the intensity of Fe^{3+}(IV)–O stretch bands in those spectra. This decreased intensity was interpreted to reflect the disappearance of tetrahedrally-coordinated ferric iron in a ferric iron-concentration range that was considerably greater than the sensitivity of the Raman spectra to Fe^{3+}(IV)–O bonds in the quenched melts (Virgo et al., 1983; Mysen et al., 1984). Further support for this suggestion is found in the values of isomer shifts of octahedrally coordinated ferric iron ($IS_{Fe^{3+}}$ = 0.4–0.65 mm/sec) in crystalline materials (Annersten and Halenius, 1976; Annersten and Olesch, 1978; Nolet and Burns, 1979; Evans and Amthauer, 1980; Huggins et al., 1975; Annersten et al., 1978; Amthauer et al., 1980). This $IS_{Fe^{3+}}$-range is similar to that of the present

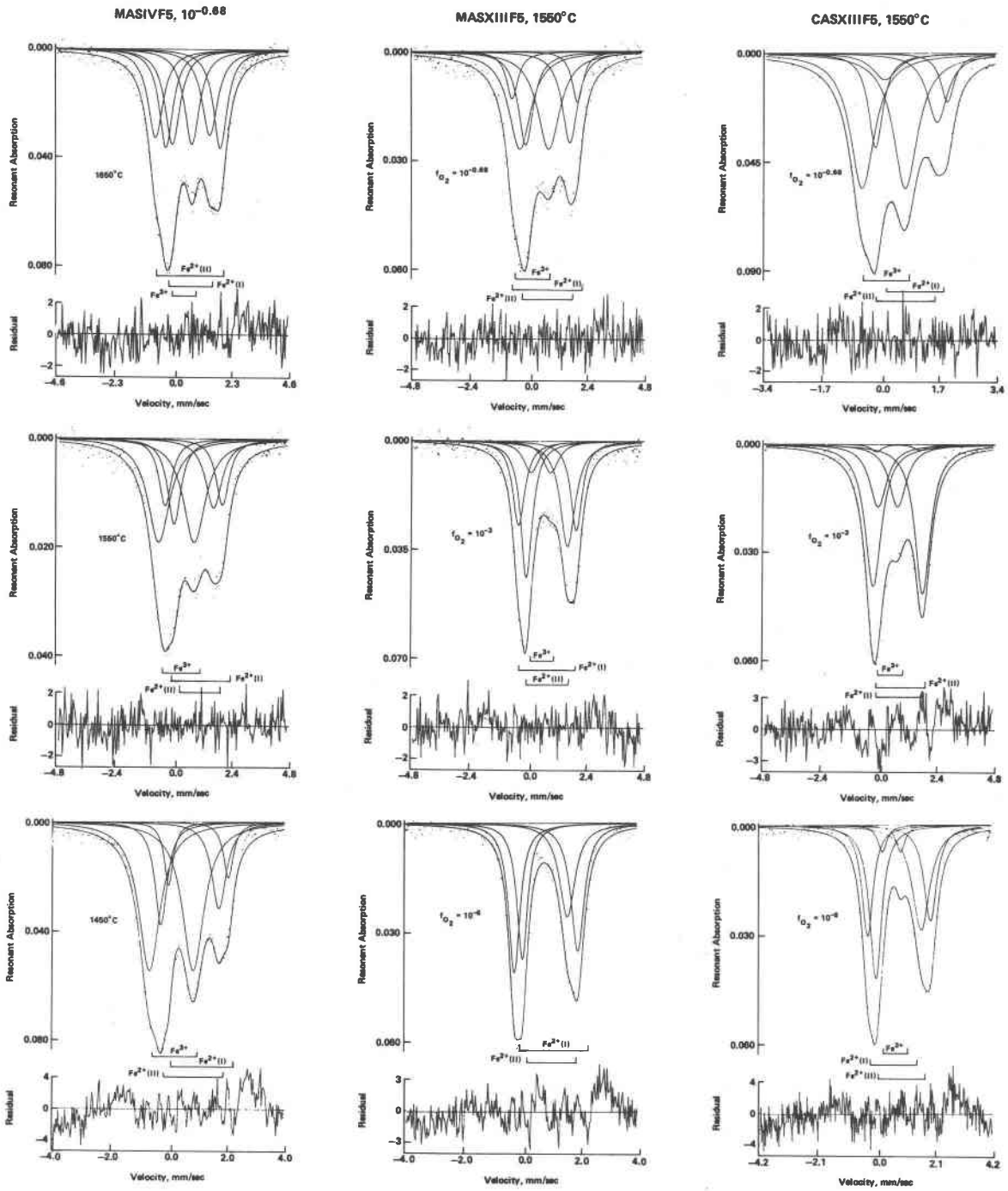

Fig. 3. Selected ^{57}Fe resonant absorption Mössbauer spectra (at 298 K) in the systems MAS and CAS. See Table 2 for details of $Fe^{3+}/\Sigma Fe$ and hyperfine parameters.

melts with $Fe^{3+}/\Sigma Fe < 0.5$. Thus, the correlation of the systematic changes of isomer shifts of ferric iron with published Raman data as well as the correlation with hyperfine parameters of octahedrally-coordinated ferric iron in crystalline materials lead to the conclusion that the gradual and systematic increase in $IS_{Fe^{3+}}$ (and decrease in $QS_{Fe^{3+}}$) as the $Fe^{3+}/\Sigma Fe$ is lowered below about 0.5 results from a coordination change of Fe^{3+} from four-fold to six-fold.

There is a ferric/ferrous range where the isomer shifts and quadrupole splitting are intermediate between about 0.3 and 0.65 mm/sec, and with continuous change in this value as a function of decreasing $Fe^{3+}/\Sigma Fe$. This behavior

Table 2. Experimental results

Comp	Temp, °C	-log f_{O_2}	Fe^{3+} IS*	Fe^{3+} QS	Fe^{2+}(I) IS	Fe^{2+}(I) QS	Fe^{2+}(II) IS	Fe^{2+}(II) QS	$Fe^{3+}/\Sigma Fe$	Fe^{2+}/Fe^{3+}
					$CaO-Al_2O_3-SiO_2-Fe-O$					
CASIF5	1625	0.68	0.291	1.319	1.079	2.142	1.026	1.594	0.556	0.678
CASIIF5	1625	0.68	0.291	1.337	1.095	2.246	1.037	1.666	0.500	1.000
CASIIIF5	1625	0.68	0.301	1.321	1.068	2.128	1.020	1.625	0.525	0.907
CASIVF5	1625	0.68	0.292	1.148	0.941	2.016	0.911	1.498	0.561	0.782
CASVF5	1625	0.68	0.289	1.363	0.997	1.924	--	--	0.711	0.406
$CASV_AF5$	1625	0.68	0.299	1.307	1.049	2.133	1.034	1.435	0.610	0.639
$CASV_B$	1625	0.68	0.327	1.265	1.094	2.205	1.024	1.674	0.564	0.773
$CASV_CF5$	1625	0.68	0.329	1.173	1.087	2.095	0.978	1.706	0.544	0.839
CASVIF5	1625	0.68	0.275	1.302	1.027	2.174	0.958	1.604	0.559	0.789
CASIF10	1625	0.68	0.236	1.454	1.040	2.200	1.005	1.244	0.446	1.245
CASIIF10	1625	0.68	0.261	1.182	1.004	1.954	0.949	1.413	0.585	0.709
CASIIIF10	1625	0.68	0.249	1.294	1.021	2.048	1.017	1.355	0.558	0.792
CASVF10	1625	0.68	0.247	1.240	0.912	1.723	--	--	0.746	0.341
CASVIF5	1575	0.68	0.276	1.416	1.062	2.242	1.022	1.556	0.568	0.759
CASIIF5	1550	0.68	0.263	1.414	1.040	2.180	1.021	1.554	0.564	0.774
CASIIIF5	1550	0.68	0.295	1.319	1.087	2.095	0.978	1.706	0.544	0.839
CASIVF5	1550	0.68	0.299	1.307	1.042	2.135	1.034	1.435	0.641	0.560
CASVF5	1550	0.68	0.275	1.377	1.172	2.010	0.923	1.807	0.759	0.317
$CASV_BF5$	1550	0.68	0.294	1.258	1.068	2.128	1.020	1.625	0.615	0.627
$CASV_CF5$	1550	0.68	0.274	1.327	1.057	2.228	1.026	1.498	0.597	0.675
CASVIF5	1550	0.68	0.278	1.282	0.970	1.914	--	--	0.749	0.336
CASVIIF5	1550	0.68	0.293	1.263	1.000	1.923	--	--	0.694	0.441
CASVIIF5†	1550	0.68	0.398	1.320	1.239	2.409	1.104	1.930	0.650	0.538
CASVIIIF5	1550	0.68	0.276	1.343	1.028	2.167	0.977	1.549	0.603	0.658
CASIXF5	1550	0.68	0.269	1.408	1.041	2.303	1.012	1.627	0.518	0.929
CASXF5	1550	0.68	0.273	1.336	0.985	1.906	--	--	0.699	0.431
CASXIF5	1550	0.68	0.278	1.291	1.050	2.231	0.989	1.534	0.679	0.472
CASXIIF5	1550	0.68	0.302	1.221	1.142	2.054	0.933	1.797	0.650	0.530
CASXIIIF5	1550	0.68	0.285	1.262	1.187	1.877	0.928	1.808	0.618	0.619
CASIVF5	1550	3.00	0.636	0.671	0.947	2.343	0.936	1.798	0.291	2.436
CASIXF5	1550	3.00	0.487	1.030	0.962	2.446	0.985	1.657	0.322	2.110
CASXIIIF5	1550	3.00	0.570	0.820	0.985	2.053	0.995	1.810	0.310	2.225
CASIVF5	1550	6.00	0.499	1.505	1.046	2.193	1.014	1.610	0.019	51.63
CASIXF5	1550	6.00	0.382	1.330	1.049	2.196	1.012	1.553	0.155	5.472
CASXIIIF5	1550	6.00	0.772	0.663	1.038	2.278	1.016	1.644	0.072	12.89
CASIVF5	1550	9.00	--	--	1.035	2.250	0.995	1.490	0.000	--
CASIVF5	1550	9.00	--	--	1.173	2.400	1.127	1.767	0.000	--
CASIXF5	1550	9.00	--	--	1.045	2.330	1.020	1.560	0.000	--
CASXIIIF5	1550	9.00	--	--	1.041	2.174	0.986	1.612	0.000	--
CASIIIF5	1500	0.68	0.305	1.287	1.024	1.909	--	--	0.647	0.545
CASIVF5	1500	0.68	0.283	1.302	0.998	1.968	--	--	0.742	0.347
CASVF5	1500	0.68	0.270	1.381	0.974	1.927	--	--	0.815	0.227
$CASV_AF5$	1500	0.68	0.295	1.286	1.018	1.947	--	--	0.685	0.439
CASIVF10	1550	0.68	0.290	1.311	0.993	1.897	--	--	0.722	0.386
CASVF10	1550	0.68	0.264	1.373	0.982	1.949	--	--	0.817	0.224
CASVF10	1550	0.68	0.247	1.331	0.938	1.916	--	--	0.863	0.158
CASIVF5	1450	0.68	0.277	1.316	0.988	1.963	--	--	0.781	0.280
CASIVF5	1450	0.68	0.392	1.357	1.137	2.147	--	--	0.754	0.327
CASIXF5	1400	0.68	0.265	1.319	1.001	1.894	--	--	0.724	0.381
CASXIIIF5	1400	0.68	0.275	1.282	1.054	2.144	0.996	1.658	0.758	0.319
CASIVF5	1400	3.00	0.370	1.171	1.162	1.962	0.864	1.944	0.470	1.128
CASIVF5	1400	6.00	0.742	0.632	1.028	2.293	1.023	1.706	0.044	21.83
CASIVF5	1400	9.00	--	--	1.021	2.162	0.994	1.600	0.000	--
					$MgO-Al_2O_3-SiO_2-Fe-O$					
MASIF5	1650	0.68	0.419	1.323	0.837	2.998	1.054	1.806	0.442	1.260
MASIIF5	1650	0.68	0.670	0.830	0.850	2.710	0.920	1.880	0.321	2.119
MASIIIF5	1650	0.68	0.470	1.230	0.900	2.710	1.020	1.750	0.350	1.850
MASIVF5	1650	0.68	0.590	0.760	0.820	2.560	0.820	1.730	0.333	1.859
MASIVF10	1650	0.68	0.290	1.320	1.010	2.080	0.850	1.490	0.490	1.026
MASVIIF5	1650	0.68	0.293	1.436	1.058	2.181	0.996	1.493	0.457	1.191
MASVIIIF5	1650	0.68	0.650	0.700	0.840	2.660	0.890	1.850	0.328	1.959
MASIXF5	1650	0.68	0.682	0.745	0.913	2.634	0.941	1.833	0.180	4.571
MASXF5	1650	0.68	0.322	1.478	1.091	2.361	1.031	1.722	0.473	1.116
MASXIF5	1650	0.68	0.434	1.139	0.830	2.621	1.031	1.802	0.401	1.495
MASXIIF5	1650	0.68	0.450	1.170	0.870	2.680	0.980	1.710	0.401	1.492
MASXIIIF5	1650	0.68	0.440	1.140	0.850	2.610	0.970	1.700	0.435	1.299
MASIIIF5	1550	0.68	0.430	1.230	0.810	2.770	0.990	1.720	0.482	1.075
MASIVF5	1550	0.68	0.423	1.307	0.892	2.906	1.025	1.819	0.511	0.958
MASVIIF5	1550	0.68	0.310	1.450	1.210	2.010	0.910	1.870	0.553	0.808
MASVIIIF5	1550	0.68	0.449	1.224	0.839	2.805	1.019	1.735	0.452	1.214
MASIXF5	1550	0.68	0.552	0.910	0.953	2.523	0.990	1.741	0.300	2.332
MASXF5	1550	0.68	0.313	1.429	1.076	2.299	1.024	1.668	0.539	0.855
MASXIF5	1550	0.68	0.440	1.245	0.834	2.874	1.028	1.778	0.478	1.093
MASXIIF5	1550	0.68	0.438	1.232	0.826	2.828	1.011	1.753	0.483	1.070
MASXIIIF5	1550	0.68	0.440	1.190	0.850	2.680	0.990	1.740	0.469	1.131
MASIVF5	1550	3.00	0.600	1.080	1.020	2.470	1.030	1.720	0.168	4.970
MASIXF5	1550	3.00	0.810	0.760	1.020	2.520	1.010	1.780	0.056	16.85
MASIXF5	1550	3.00	0.900	0.870	1.180	2.650	1.140	1.720	0.078	11.83
MASXIIIF5	1550	3.00	0.589	1.068	1.040	2.347	1.014	1.677	0.188	4.319
MASIVF5	1550	6.00	--	--	1.070	2.240	1.030	1.570	0.000	--
MASIVF5	1550	6.00	--	--	1.210	2.480	1.160	1.770	0.000	--
MASIXF5	1550	6.00	--	--	1.080	2.400	1.050	1.640	0.000	--
MASXIIIF5	1550	6.00	--	--	1.070	2.220	1.040	1.610	0.000	--
MASIVF5	1550	9.00	--	--	1.080	2.280	0.990	1.620	0.000	--
MASIVF5	1550	9.00	--	--	1.210	2.460	1.160	1.770	0.000	--
MASIXF5	1550	9.00	--	--	1.100	2.270	1.160	1.620	0.000	--
MASXIIIF5	1550	9.00	--	--	1.065	1.970	0.880	1.830	0.000	--
MASIVF5	1450	0.68	0.300	1.490	1.210	2.010	0.910	1.890	0.573	0.744
MASIVF10	1450	0.68	0.300	1.400	1.040	1.970	--	--	0.674	0.483

*Isomer shifts (IS) at quadrupole splitting (QS) in mm/sec relative to Fe metal.
†Underlining denotes spectrum taken at 77 K.

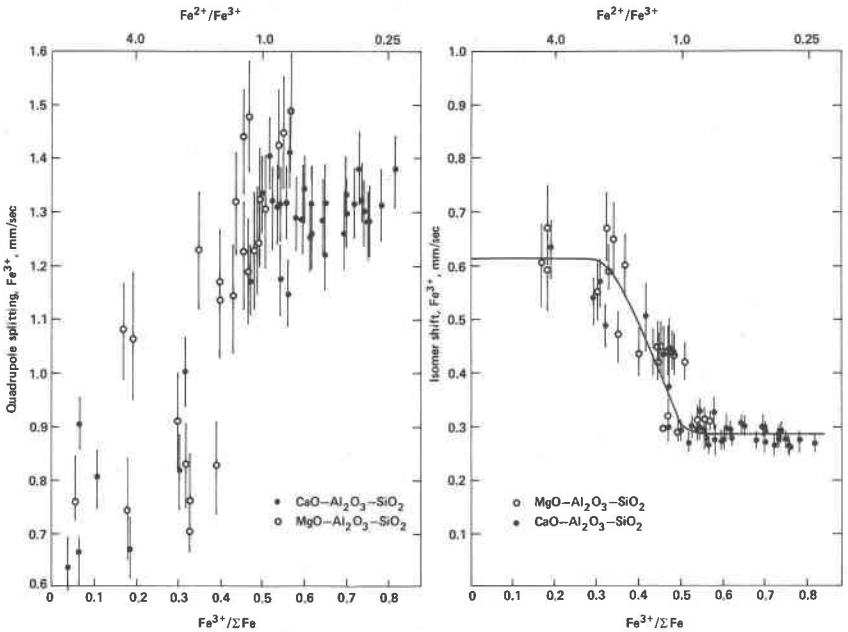

Fig. 4 Variations in hyperfine parameters (quadrupole splitting and isomer shift) in the systems $MgO–Al_2O_3–SiO_2–Fe–O$ (open circles) and $CaO–Al_2O_3–SiO_2–Fe–O$ (closed circles) as a function of measured $Fe^{3+}/\Sigma Fe$. Isomer shifts are relative to Fe metal.

could be the result of coexisting tetrahedral and octahedral ferric iron, or it could be the result of localized electron hopping between adjacent "sites" for Fe^{2+} and Fe^{3+} as observed, for example, in the Mössbauer spectra of some iron-bearing silicate minerals (e.g., Nolet and Burns, 1979; Amthauer et al., 1980; Coey et al., 1982). Localized electron hopping is, however, inconsistent with the observed temperature-independence of the ferric doublet (see Table 2, additional discussion will be presented by Virgo and Mysen, 1985). Moreover, as noted above, in melts in the system $Na_2O–Al_2O_3–SiO_2–Fe–O$, two ferric doublets could be fitted in the spectra from samples in this intermediate $Fe^{3+}/\Sigma Fe$-range. One doublet resulted in hyperfine parameters consistent with tetrahedrally-coordinated Fe^{3+} and one with octahedrally-coordinated Fe^{3+} (Virgo and Mysen, 1985). In the alkaline earth aluminosilicate samples discussed here, there is a significant broadening of the component peaks of the fitted ferric iron doublet in the $Fe^{3+}/\Sigma Fe$ range between 0.5 and 0.3, a broadening that is consistent with the existence of at least two ferric doublets. The resolution of the Mössbauer spectra of these samples does not appear, however, to permit a fit without severe constraints (quadrupole split).

It is concluded, therefore, that in highly oxidized ($Fe^{3+}/\Sigma Fe > 0.5$) aluminosilicate melts with Ca^{2+} or Mg^{2+} for electrical charge-balance, ferric iron is in tetrahedral coordination. Similar observations have been made for melts in the systems $Na_2O–SiO_2–Fe–O$ (Virgo et al., 1982, 1983), $CaO–SiO_2–Fe–O$, $MgO–SiO_2–Fe–O$ (Mysen et al., 1984) and $Na_2O–Al_2O_3–SiO_2–Fe–O$ (Mysen and Virgo, 1983a; Virgo and Mysen, 1985). From the Raman spectra of the alkali and alkaline earth silicate melts, the Raman spectra indicate that this ferric iron was highly ordered (either constant Si/Fe^{3+}, or no Si in those tetrahedra). Similar conclusions may apply to the aluminosilicate systems.

In all systems and with different iron contents, a gradual increase in $IS_{Fe^{3+}}$ (and a decrease in $QS_{Fe^{3+}}$) began to take place with $Fe^{3+}/\Sigma Fe$ decreasing below 0.5. This latter observation leads to the conclusion that the coordination transformation of ferric iron appears tied to the relative proportion of ferric and ferrous iron in the melts. Thus, a melt complex involving an association between these two cations (e.g., Fe_3O_4) may be suggested. Magnetic properties of glasses in the system $CaO–SiO_2–Fe–O$ as a function of $Fe^{3+}/\Sigma Fe$ (O'Horo and Levy, 1978) are also consistent with this suggestion. As additional ferrous iron is formed with further reduction of $Fe^{3+}/\Sigma Fe$, this additional Fe^{2+} most likely occurs as a network-modifying cation linking the non-bridging oxygens in the various coexisting units.

Ferrous iron is commonly considered to be a network modifier in silicate melts. Coordination polyhedra with six oxygens are consistent with the values of isomer shifts and quadrupole splitting of both ferrous iron doublets (e.g., Mao et al., 1973; Bell and Mao, 1974; Nolet et al., 1979; Mysen and Virgo, 1978; Calas and Petiau, 1983; Mysen et al., 1980a).

Redox relations

The Fe^{2+}/Fe^{3+} values are positively correlated with decreasing NBO/T and Al/(Al + Si) at the same temperature and oxygen fugacity (Fig. 5). Similar correlations have been

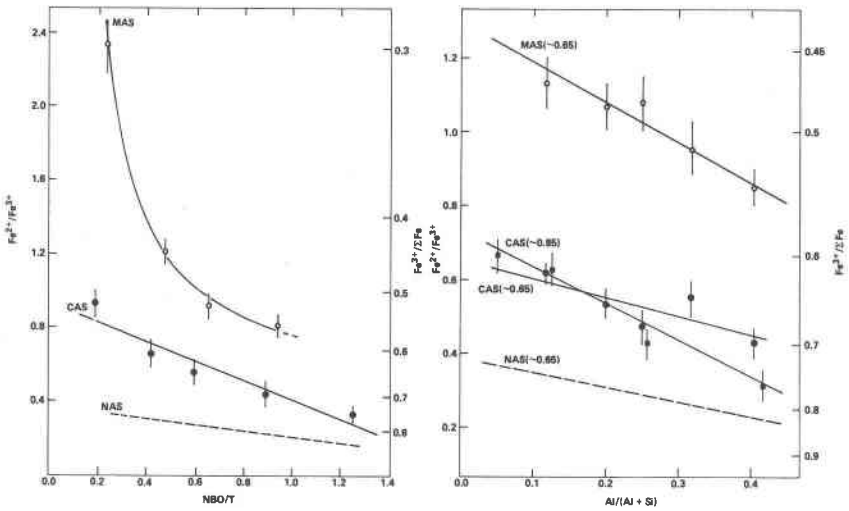

Fig. 5. The Fe^{2+}/Fe^{3+} of quenched melts in the systems $CaO–Al_2O_3–SiO_2–Fe–O$ (CAS) and $MgO–Al_2O_3–SiO_2–Fe–O$ (MAS) as a function of NBO/T at Al/(Al + Si) = 0.334 and as a function of Al/(Al + Si) at indicated NBO/T with 5 wt.% iron oxide added as Fe_2O_3 and equilibrated in air at 1550°C.

reported from several Al-free alkali and alkaline earth silicate systems (e.g., Larson and Chipman, 1953; Paul and Douglas, 1965; Goldman, 1983; Mysen et al., 1984). There is a near linear relation between redox ratio and NBO/T in the NBO/T range between about 0.3 and 1.0 (see also Fig. 5) in both the system $CaO–Al_2O_3–SiO_2–Fe–O$ and the system $Na_2O–Al_2O_3–SiO_2–Fe–O$ (data also from Mysen and Virgo, 1983a; Virgon and Mysen, 1985). In the $MgO–Al_2O_3–SiO_2–Fe–O$ system the linear correlation between Fe^{2+}/Fe^{3+} and NBO/T obtained for Ca- and Na-aluminosilicate glasses no longer exists (Fig. 5). This different behavior of the Fe^{2+}/Fe^{3+} versus NBO/T results from the fact that even for MAS melts with NBO/T < 0.4 equilibrated with air at 1550°C, the $Fe^{3+}/\Sigma Fe$ is less than 0.5, and some of the ferric iron no longer is in tetrahedral coordination. Inasmuch as the activity coefficients of Fe^{3+}(IV) and Fe^{3+}(VI) most likely differ from each other, the Fe^{2+}/Fe^{3+} will depend on $Fe^{3+}(IV)/Fe^{3+}(VI)$ as also indicated by the data in Figure 5.

In the Al-free alkali- and alkaline-earth-bearing end-member systems the Fe^{2+}/Fe^{3+} is a linear function of Z/r^2 (ionization potential) of the alkaline earth and alkali metal cation (Mysen et al., 1984), and NBO/T has no apparent effect on this relationship. In the present, aluminous systems, the Fe^{2+}/Fe^{3+} also increases with increasing Z/r^2 (Fig. 6), but the relationship is distinctly nonlinear and the dependence of Fe^{2+}/Fe^{3+} on Z/r^2 is more pronounced the more polymerized the melt (smaller NBO/T).

With ferric iron in tetrahedral coordination, log (Fe^{2+}/Fe^{3+}) is linearly correlated with $1/T$ (absolute temperature) and $\log f_{O_2}$ (Figs. 7 and 8). The nonlinearity of the MASIVF5 curve (Fig. 7c) results from a coordination transformation of Fe^{3+} in this composition as the temperature is increased from 1550° to 1650°C (see Table 2).

For melts with Fe^{3+}(IV) and Fe^{2+}(VI), the Fe^{2+}/Fe^{3+} decreases with decreasing degree of polymerization (increasing NBO/T) of the melts (e.g., Larson and Chipman, 1953; Douglas et al., 1965; Virgo et al., 1982; Goldman, 1983; Mysen et al., 1984). As a result, it has been suggested (Holmquist, 1966; see also Goldman, 1983) that the redox equilibria may be illustrated with a simplified expression of the form:

$$4Fe(IV)O_2^- = 4Fe^{2+}(VI) + 6O^{2-} + O_2. \qquad (1)$$

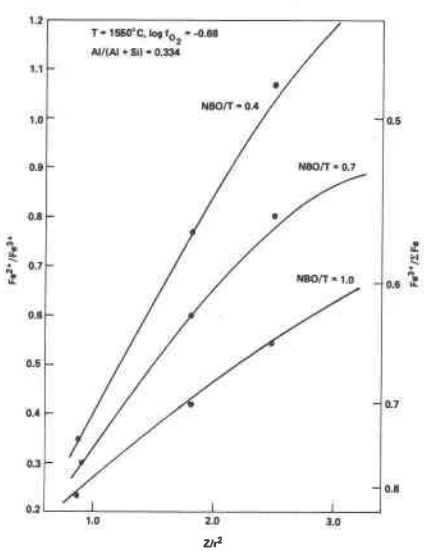

Fig. 6. The Fe^{2+}/Fe^{3+} of melts in the systems $Na_2O–Al_2O_3–SiO_2–Fe–O$, $CaO–Al_2O_3–SiO_2–Fe–O$ and $MgO–Al_2O_3–SiO_2–Fe–O$ expressed as Z/r^2 of the alkali and alkaline earth cation as a function of bulk melt NBO/T at 1550°C and the oxygen fugacity of air. (Data for the system NAS from Mysen and Virgo, 1983a; Virgo and Mysen, 1985.)

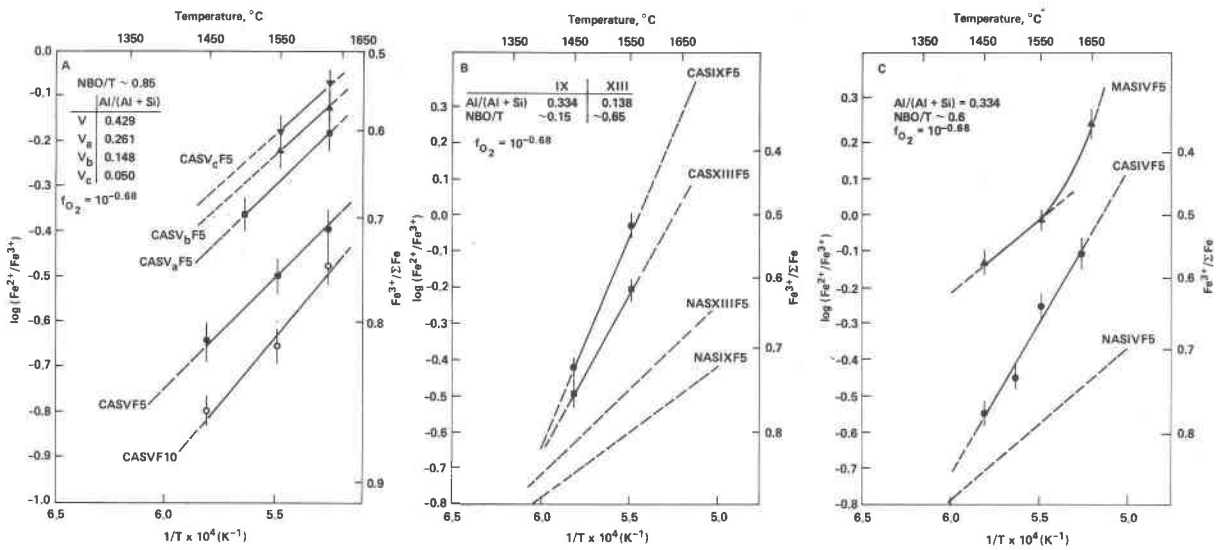

Fig. 7. Log (Fe^{2+}/Fe^{3+}) vs. $1/T$ (K) as a function of type of metal cation at constant NBO/T and Al/(Al + Si); as a function of Al/(Al + Si) with the same metal cation and NBO/T; and as a function of NBO/T with constant Al/(Al + Si) and metal cation. Dashed lines for NAS obtained from data for the system Na_2O–Al_2O_3–SiO_2–Fe–O (Mysen and Virgo, 1983a; Virgo and Mysen, in prep.).

With the assumption of a linear relationship the standard-state free energy of reduction of ferric to ferrous iron expressed with equation (1) can be estimated as the lines (Fig. 7) conform to the expression

$$\ln K = -\Delta G^0/RT, \qquad (2)$$

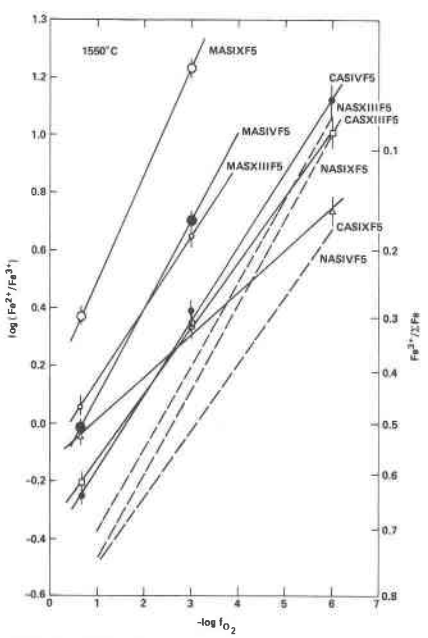

Fig. 8. Relationships between redox ratios and oxygen fugacity at 1550°C as a function of the same bulk compositional variables as the data in Fig. 7. Dashed lines for system Na_2O–Al_2O_3–SiO_2–Fe–O are from Mysen and Virgo (1983a) and Virgo and Mysen (1985).

where the equilibrium constant, K, is that of equation (1). Strictly speaking, the concentration ratio, Fe^{2+}/Fe^{3+} should be the activity ratio, $a_{Fe^{2+}}/a_{Fe^{3+}}$. The linear relationship between log (Fe^{2+}/Fe^{3+}) and $1/T$ indicates, however, that the activity coefficient ratio, $\gamma_{Fe^{2+}}/\gamma_{Fe^{3+}}$, is temperature independent in the temperature-range studied here. The standard free energies of reduction are given in Table 3. It is evident that at the same NBO/T and Al/(Al + Si), the ΔG^o of reduction is greater for Ca-aluminosilicate melts than for Na-aluminosilicate melts with Fe^{3+} in tetrahedral coordination and Fe^{2+} in octahedral coordination. Furthermore, the free-energy changes decrease with decreasing bulk melt NBO/T and with decreasing Al/(Al + Si) for both Na and Ca systems. The relationship of ΔG^o to Al/(Al + Si) is less pronounced for higher values of bulk melt NBO/T (Table 3).

There is a near linear relation between log (Fe^{2+}/Fe^{3+})

Table 3. Standard free energies of reduction (kcal/mol) of ferric to ferrous iron

Composition	NBO/T*	Al/(Al + Si)	$\Delta G°$
CASIVF5	0.65	0.334	7.7
CASXIIIF5	0.65	0.138	5.1
CASIXF5	0.17	0.334	6.9
CASVF5	0.85	0.429	5.7
$CASV_AF5$	0.85	0.261	3.8
$CASV_BF5$	0.85	0.148	3.7
$CASV_CF5$	0.85	0.050	3.8
CASVF10	0.85	0.529	7.7
NASIVF5†	0.65	0.334	3.9
NASIXF5†	0.17	0.334	2.1
NASXIIIF5	0.65	0.138	3.4

*Nonbridging oxygens per tetrahedral cations in the iron-free end-member system.
†Data from Mysen and Virgo (1983a).

and log f_{O_2} (Fig. 8). Similar relationships have been obtained in complex natural magmatic liquids (e.g., Thornber et al., 1980) as well as in numerous simpler binary and ternary silicate systems (e.g., Seifert et al., 1979; Goldman, 1983; Virgo et al., 1983; Mysen et al., 1984). In contrast to Na-bearing systems, where the slopes of the log f_{O_2} vs. log (Fe^{2+}/Fe^{3+}) are about -0.25 for a range of bulk melt NBO/T values, in the alkaline earth aluminosilicate melt systems the slopes range from -0.15 to -0.37. The slopes generally become steeper with increasing Z/r^2 of the alkaline earth cation. No clear trend emerges for the relations between NBO/T or Al/(Al + Si) and the slopes of the redox curves. This observation differs from the data reported in the Al-free end-member system, where, for example, the absolute value of the slope increases with decreasing bulk melt NBO/T (Mysen et al., 1984). Evidently, this simple relationship is affected by the presence of significant proportions of Al^{3+} in the melts.

Discussion

Polymerization and redox equilibria

Ferrous iron is a network modifier in the silicate melts studied here. Ferric iron, on the other hand, can be both a network former and a network modifier. Its coordination polyhedron is principally a function of $Fe^{3+}/\Sigma Fe$. The degree of polymerization (NBO/T) of the iron-bearing silicate melt depends, therefore, on the same intensive and extensive variables that affect $Fe^{3+}/\Sigma Fe$. A possible exception to this rule may be peralkaline aluminosilicate melts where Dickenson and Hess (1981) found Fe^{2+}/Fe^{3+} to be essentially independent of NBO/T. Some calculations used to illustrate the extent of changes of NBO/T in the systems Na_2O–Al_2O_3–SiO_2 (Mysen and Virgo, 1983a; Virgo and Mysen, 1985), CaO–Al_2O_3–SiO_2 and MgO–Al_2O_3–SiO_2 are shown in Figure 9.

The $Fe^{3+}/\Sigma Fe$ is a simple function of temperature (Fig. 7). Thus, the NBO/T (degree of polymerization) of melts in the systems NAS, CAS and MAS at the same Al/(Al + Si) and oxygen fugacity increases with increasing temperature. Because the bulk melt NBO/T increases with decreasing $Fe^{3+}/\Sigma Fe$ as long as Fe^{3+} is in four-fold and Fe^{2+} is in six-fold coordination, the NBO/T will increase with increasing temperature, with decreasing f_{O_2} and with decreasing Al/(Al + Si). Inasmuch as the temperature dependence of $Fe^{3+}/\Sigma Fe$ is greater the greater the Z/r^2 of the alkaline earth or alkali metal cation, the NBO/T of iron-bearing melts becomes more distinctly dependent on the type of metal cation in the order Na < Ca < Mg.

Lowering of the oxygen fugacity reduces the $Fe^{3+}/\Sigma Fe$ and thus results in enhancement of NBO/T. For the three systems MgO–Al_2O_3–SiO_2–Fe–O, CaO–Al_2O_3–SiO_2–Fe–O and Na_2O–Al_2O_3–SiO_2–Fe–O at 1550°C, Fe^{3+} will undergo a coordination transformation at some f_{O_2} less than that of air (Figs. 4 and 8). It can be seen from the results in Figure 9B that the NBO/T changes by as much as 15–25% as a function of decreasing f_{O_2}. The change of slopes of the curves in Figure 9 and eventual transition

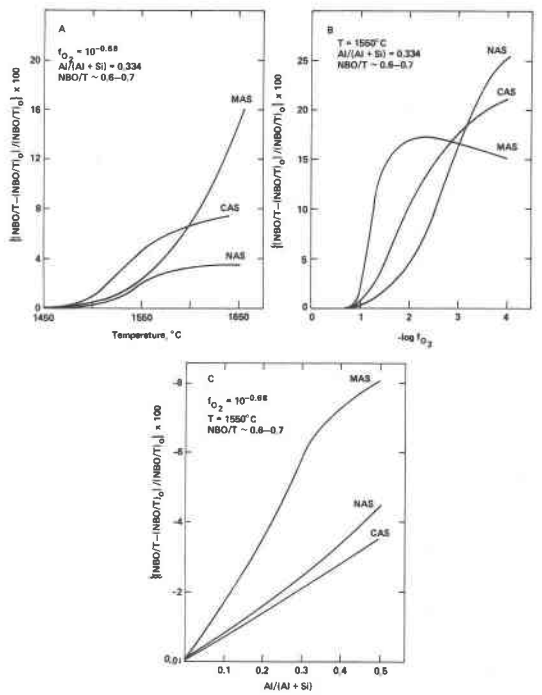

Fig. 9. Variations in melt polymerization (NBO/T) as a function of $Fe^{3+}/\Sigma Fe$ calculated as a function of temperature (A), oxygen fugacity (B) and Al/(Al + Si) (C). Reference points, $(NBO/T)_0$, are at 1450°C (A), $-\log f_{O_2} = 0.68$ (air) (B) and Al/(Al + Si) = 0.0 (C).

from an increase to a decrease in NBO/T with decreasing f_{O_2} stem from the gradual coordination transformation of ferric iron from IV-fold to VI-fold coordination. This apparent contrast in the functional relations between NBO/T and $Fe^{3+}/\Sigma Fe$ for Fe^{3+}(IV) and Fe^{3+}(VI) results from the fact that with Fe^{3+} in octahedral coordination, the redox equilibrium may be illustrated with the formalized expression;

$$Fe^{3+}(VI) + O^- = Fe^{2+}(VI) + 1/2O_2, \qquad (3)$$

where O^- is nonbridging oxygen in the silicate network. Consequently, increasing $Fe^{3+}/\Sigma Fe$ at constant f_{O_2} requires a decreasing activity of the nonbridging oxygen. That is to say, the bulk melt NBO/T will, in fact, decrease as the result of reducing Fe^{3+}(VI) to Fe^{2+}(VI). This transition is more rapid in the system MAS than in CAS and more rapid in CAS than in NAS.

The negative (and generally linear) correlation between Fe^{2+}/Fe^{3+} and Al/(Al + Si) also results in increasing bulk melt NBO/T as a function of decreasing Al/(Al + Si). Consequently, even though the structural positions of Al^{3+} and Si^{4+} in aluminosilicate melts most probably remain unaltered by the changes in Al/(Al + Si) (divalent metal cations charge-balance Al^{3+} in four-fold coordination), the bulk melt NBO/T of the iron-bearing MAS, CAS and NAS samples decreases systematically with increasing Al/(Al

+ Si). Inasmuch as $Fe^{3+}/\Sigma Fe$ is more sensitive to Al/(Al + Si) in the iron-bearing magnesium aluminosilicate system than in the other systems (Fig. 5), the NBO/T variations resulting from the change in $Fe^{3+}/\Sigma Fe$ are also more sensitive to Al/(Al + Si) in the system $MgO–Al_2O_3–SiO_2–Fe–O$ than in the systems $CaO–Al_2O_3–SiO_2–Fe–O$ and $Na_2O–Al_2O_3–SiO_2–Fe–O$ (Fig. 9).

Liquidus equilibria and the structure of iron-bearing aluminosilicate melts

Liquidus phase-equilibrium relations and melt–mineral element partitioning depend on the bulk compositions (structure) of both the mineral and the coexisting liquid. For example, a survey of REE partition coefficients between garnet and magmatic liquids (Irving and Frey, 1978) indicates that the partition coefficients may vary by more than an order of magnitude as a function of magma composition alone. Compositional variables, recast to atomic ratios such as Si/O of the melt, have been used to obtain a correlation between this ratio and partition coefficients between olivine and such melts (Watson, 1977; Hart and Davis, 1978). The Si/O is a simplified expression of melt polymerization, but does not take into account other tetrahedrally coordinated cations (e.g., Al^{3+}, Fe^{3+}, P^{5+} and Ti^{4+}), distribution of such cations between different structural units in the melt (e.g., Mysen et al., 1981, 1982b, 1985) and the possible complexing of the trace element with specific elements in the melt (Watson, 1976; Ryerson and Hess, 1980). It has been found for Ni, Mn and several REE that the polymerization parameter, NBO/T, which does not, however, consider cation distribution or complexing, is linearly correlated with olivine–liquid and diopside–liquid partition coefficients in aluminosilicate systems such as $CaMgSi_2O_6–NaAlSiO_4–SiO_2$ and $Mg_2SiO_4–NaAlSi_3O_8–CaAl_2Si_2O_8$ (Mysen and Virgo, 1980). The linear correlations at constant temperature are valid whether or not Ca^{2+}, Mg^{2+} or Na^+ acts as a charge-balancing cation of tetrahedrally coordinated Al^{3+} at least in the NBO/T range from 0.2–1.0.

One may therefore relate changes in melt–mineral partition coefficients that result from the relationship between redox ratio and NBO/T of the melt to intensive and extensive variables that govern the values of $Fe^{3+}/\Sigma Fe$ (Fig. 9). For example, the variations in NBO/T as a function of f_{O_2} or Al/(Al + Si) with 5 wt.% iron added as Fe_2O_3 to a melt with NBO/T = 0.6 are well within the NBO/T ranges of linear correlation between partition coefficients and NBO/T in the systems summarized by Mysen and Virgo (1980). As mentioned briefly above [see equation (1)], ferric iron as a network former most likely forms separate ferrite complexes (Fox et al., 1982; Virgo et al., 1982; Mysen et al., 1984). These complexes may be described with the generalized expression $FeO_n^{(3-2n)+}$ (Holmquist, 1966; Goldman, 1983). Virgo et al. (1982) and Mysen and Virgo (1983b) concluded from Mössbauer and Raman data that most likely n = 2 in alkali and alkaline earth silicate melts. Virgo et al. (1982) concluded from the Raman data, for example, that the character of this complex does not depend on the amount of tetrahedrally-coordinated Fe^{3+}. Only the relative abundance of the ferrite complex changes with ferric iron concentration. The relative abundance of FeO_2^- complexes (which are analogous to the three-dimensionally-interconnected aluminate or silicate complexes found in these and other melts) in a melt will affect the bulk melt NBO/T but not the character of the bridging and nonbridging oxygens in the silicate anionic units. Equation (1) may be combined with any polymerization reaction for the silicate such as, for example;

$$SiO_3^{2-} = SiO_2 + O^{2-}, \qquad (4)$$

to illustrate the relationship between $Fe^{3+}(IV) \rightarrow Fe^{2+}(VI)$ and the NBO/T of the melt:

$$6SiO_3^{2-}(2) + 4Fe^{2+}(VI) + O_2 = 6SiO_2(0) + 4Fe(IV)O_2^-. \qquad (5)$$

In equation (5), the numbers in parentheses represent the NBO/T (or NBO/Si) of that particular melt structural unit. The Roman numerals represent the oxygen coordination number around Fe^{3+} and Fe^{2+}.

The changes in olivine–liquid Ni and Mn partition coefficients in the system $Mg_2SiO_4–NaAlSi_3O_8–CaAl_2Si_2O_8$ at 1550°C have been calculated (Fig. 10). The Ni and Mn data are from Hart and Davis (1978) and Watson (1977), respectively. The 1550°C results are calculated by extrapolation of partition coefficients that are linearly correlated (r is a correlation coefficient) with NBO/T at constant temperature from 1250°C to 1450°C. The correlations at the different temperatures are as follows:

K_{Ni}^{ol-liq} (Hart and Davis, 1978):

$$1250°C: K = -24.1(NBO/T) + 23.6, \; r = 0.95, \qquad (6)$$

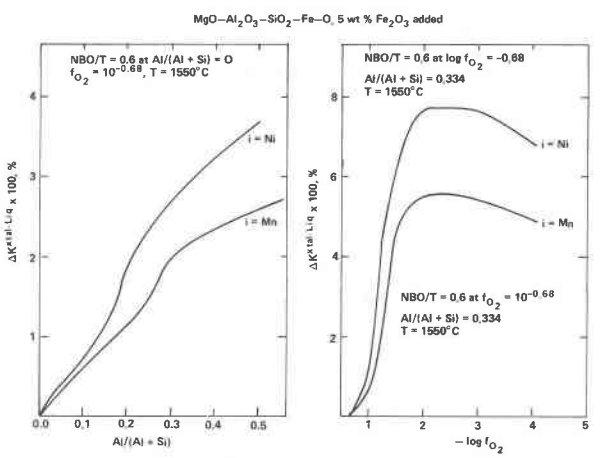

Fig. 10. Calculated changes in hypothetical olivine–liquid manganese and nickel partition coefficients in the system $MgO–Al_2O_3–SiO_2–Fe–O$ with 5 wt.% iron oxide added as Fe_2O_3 relative to values at Al/(Al + Si) = 0.0 and $-\log f_{O_2} = 0.68$, respectively. Base element partitioning data from Watson (1977) and Hart and Davis (1978). See text for details of data extrapolation.

$$1350°C: K = -12.4(NBO/T) + 15.9, r = 0.97, \quad (7)$$

$$1450°C: K = -5.11(NBO/T) + 0.77, r = 0.98, \quad (8)$$

which at 1550°C yields

$$1550°C: K = -4.52(NBO/T) + 8.72, r = 0.99. \quad (9)$$

K_{Mn}^{ol-liq} (Watson, 1977):

$$1300°C: K = -1.02(NBO/T) + 1.59, r = 0.91, \quad (10)$$

$$1350°C: K = -1.10(NBO/T) + 1.62, r = 0.96, \quad (11)$$

$$1450°C: K = -0.59(NBO/T) + 1.23, r = 0.98, \quad (12)$$

which at 1550° yields

$$1550°C: K = -0.44(NBO/T) + 1.08, r = 0.99, \quad (13)$$

The calculated examples (Fig. 10) are for the end-member system $MgO–Al_2O_3–SiO_2$ with NBO/T about 0.6. Five wt.% iron oxide as Fe_2O_3 was used in the calculations. The relationships between $Fe^{3+}/\Sigma Fe$, f_{O_2} and Al/(Al + Si) (Figs. 5 and 8) were used to calculate the NBO/T and thus the changes in $K_i^{xtal-liq}$ as a function of Al/(Al + Si) and f_{O_2}. For this amount of total iron, changes in Al/(Al + Si) alone have a real but relatively small effect on the partition coefficients in the range Al/(Al + Si) = 0–0.5. At lower temperature, or with more iron added to the system (e.g., as found in natural basaltic liquid), the influence of Al/(Al + Si) on the partition coefficients will be enhanced because the partition coefficients are more dependent on NBO/T at lower temperature.

The changes in partition coefficients with f_{O_2} were calculated relative to the value of $Fe^{3+}/\Sigma Fe$ in melts equilibrated with air at 1550°C. A reduction of the oxygen fugacity by approximately two orders of magnitude results in a transformation of all Fe^{3+} from tetrahedral to octahedral coordination, under which conditions the NBO/T of the melt reaches a maximum value. This maximum corresponds to about an 8% decrease in the value of the partition coefficients. At lower temperatures, where $Fe^{3+}/\Sigma Fe$ may be more sensitive to f_{O_2} and the partition coefficients are more strongly temperature dependent, with iron contents comparable to those of basalt, the effect of f_{O_2} on the partition coefficients may be more than twice that shown in Figure 10. Thus, oxygen fugacity significantly affects the crystal–liquid element partitioning of transition elements such as Mn and Ni even though the oxidation states of the transition elements themselves may not be affected.

The liquidus phase equilibria of Fe-free minerals in iron-bearing aluminosilicate systems can be correlated with the structure of the coexisting iron-bearing aluminosilicate melt. A few calculated examples of liquidus equilibria in the systems $CaO–Al_2O_3–SiO_2$ and $MgO–Al_2O_3–SiO_2$ with 10 wt.% iron oxide added (in the calculations) as Fe_2O_3 are shown in Figure 11. The composition of the iron-free melt used in this calculation is defined by the intersection of the line Al/(Al + Si) = 0.2 with the metasilicate–tectosilicate liquidus boundary (Fig. 11). The NBO/T of melts along the line Al/(Al + Si) = 0.2 (labeled *a* in Fig. 11E and F) as a function of $Fe^{3+}/\Sigma Fe$ and coordination of Fe^{3+} was calculated. The NBO/T at Al/(Al + Si) = 0.2 was then projected into the ternary composition plane, and the phase equilibria were derived from the published data (Osborn and Muan, 1960a,d). The compositions thus projected will move along the line Al/(Al + Si) = 0.2 as defined by the total iron content and $Fe^{3+}/\Sigma Fe$.

In both systems the addition of 10 wt.% Fe_2O_3 shifts the composition from the metasilicate–tectosilicate liquidus boundary into the liquidus field of a silica polymorph. The temperatures are between 70° and 100°C higher than those at the liquidus boundaries of the iron-free compositions. The metasilicate–tectosilicate liquidus boundary is reached at $Fe^{3+}/\Sigma Fe$ between 0.65 and 0.45. This liquidus boundary is encountered at a greater value of NBO/T and, thus, at higher $Fe^{3+}/\Sigma Fe$ in the system CAS than in the system MAS. This difference probably results from the greater dispersion of anionic units in magnesium aluminosilicate than in calcium aluminosilicate melts (see Liebau, 1981; Mysen et al., 1982a,b). That is, even at the same bulk melt NBO/T, the abundance of SiO_3^{2-} and SiO_2 units relative to $Si_2O_5^{2-}$ units is greater in the magnesium system than in the calcium system. Such differences are consistent with the melt structure data in the systems $CaO–SiO_2$ and $MgO–SiO_2$ (Mysen et al., 1982a). This liquidus boundary represents a minimum temperature as further lowering of $Fe^{3+}/\Sigma Fe$ is manifested by metasilicate on the liquidus with increasing thermal stability. The steeper slope of the liquidus surface in the Ca system is a direct consequence of the topology of the liquidus surface of pseudowollastonite in the system $CaO–Al_2O_3–SiO_2$ (Osborn and Muan, 1960a,d). The inflection of the metasilicate liquidus surfaces and thermal maximum at $Fe^{3+}/\Sigma Fe \sim 0.3$ (Fig. 11A and B) is due to the coordination transformation of Fe^{3+}. This transformation results in a maximum value of NBO/T at this $Fe^{3+}/\Sigma Fe$ and thus the topological features shown in Figure 11. The dashed lines [denoted Fe^{3+}(IV)] represent the slopes of the metasilicate liquidi calculated for a hypothetical situation with Fe^{3+} in tetrahedral coordination in the entire $Fe^{3+}/\Sigma Fe$ range.

The liquidus phase equilibria in these systems may also be displayed as a function of recalculated Al/(Al + Si) along lines of constant $Fe^{3+}/\Sigma Fe$ and, therefore, constant NBO/T. The shaded areas in Figure 11 (E and F) represent the compositional ranges obtained by adding 10 wt.% iron oxide as Fe_2O_3 with $Fe^{3+}/\Sigma Fe$ between 1.0 and 0.0 to aluminosilicate melts with NBO/T = 0.6. The topologies of the liquidus surfaces along composition lines with $Fe^{3+}/\Sigma Fe$ = 1.0, 0.5 and 0.0 are also shown in Figure 11 (C and D).

The addition of ferric iron, and a concomitant increase in polymerization (from NBO/T = 0.6 to ~0.42), result in an increase in the liquidus temperature relative to the iron-free solvent across most of the Al/(Al + Si) range (0.0–0.5) (Fig. 11C and D). A silica polymorph is on the liquidus to Al/(Al + Si) $\geqq$ 0.1. For a given $Fe^{3+}/\Sigma Fe$, this range in Al/(Al + Si) is 30–60% wider in the magnesium aluminosilicate system than in the calcium aluminosilicate system.

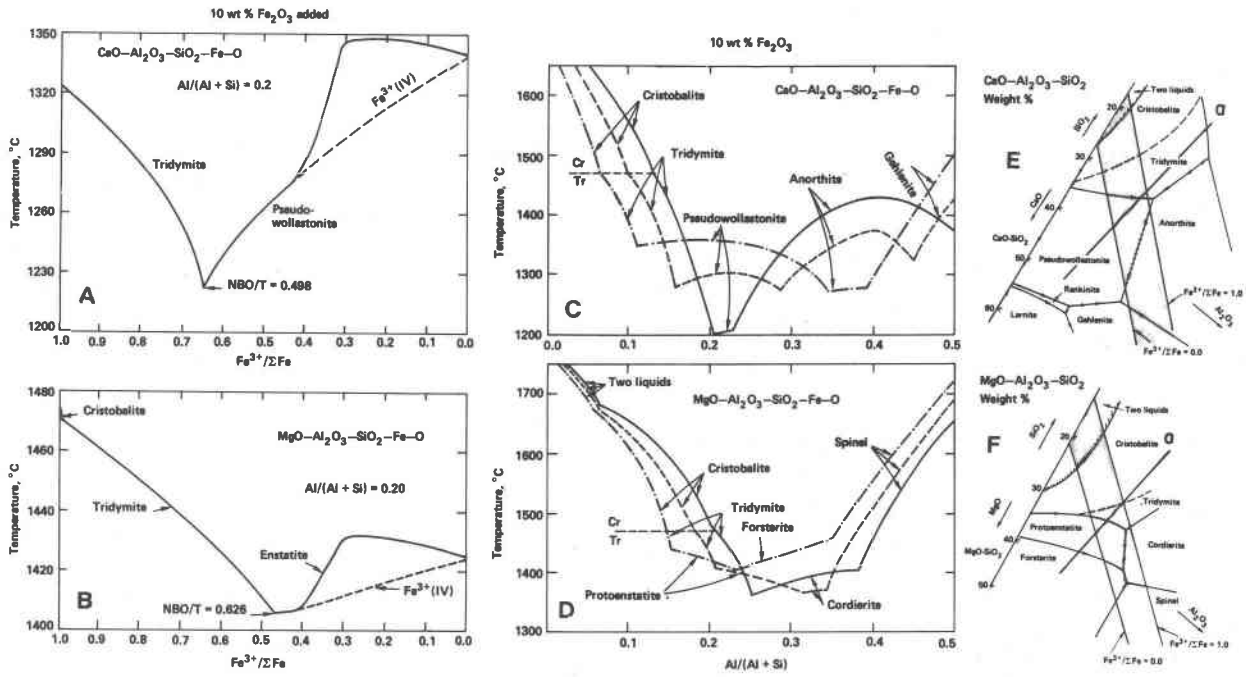

Fig. 11. Calculated liquidus phase equilibria at 1 atm pressure in the systems $CaO–Al_2O_3–SiO_2–Fe–O$ and $MgO–Al_2O_3–SiO_2–Fe–O$ with 10 wt.% iron oxide added as Fe_2O_3. In C and D the solid line denotes $Fe^{3+}/\Sigma Fe = 1.0$; dashed line, $Fe^{3+}/\Sigma Fe = 0.5$; dot-dashed line, $Fe^{3+}/\Sigma Fe = 0.0$. In E and F the line labeled *a* denotes Al/(Al + Si) = 0.2. See text for additional details.

The value of Al/(Al + Si) at the tectosilicate–metasilicate liquidus boundary decreases and the temperature increases as ferric iron is reduced to ferrous iron (Fig. 11C and D). These changes result from the increased bulk melt NBO/T with reduction of Fe^{3+} to Fe^{2+}. This same reduction in $Fe^{3+}/\Sigma Fe$ is also accompanied by rapid expansion of the metasilicate liquidus volume in the calcium system and by the appearance of orthosilicate (forsterite) in the magnesium system. There is no aluminosilicate liquidus phase in the magnesium system, and spinel is a liquidus phase as the Al/(Al + Si) is increased further. In the calcium aluminosilicate system, a further increase in Al/(Al + Si) results in the appearance of anorthite with a thermal maximum on the liquidus surface. Thus, merely increasing Al/(Al + Si) at constant NBO/T of the melt results in a transition first from a tectosilicate to a metasilicate liquidus phase (decreased polymerization of the liquidus phase), then to a completely polymerized aluminosilicate phase. The liquidus volume of anorthite shrinks with further reduction of ferric iron. Finally, the highly depolymerized pyrosilicate, gehlenite, instead of anorthtite, occurs on the liquidus for compositions with nearly all iron as Fe^{2+} and Al/(Al + Si) about 0.5. Mysen et al. (1982a,b, 1985) noted the existence of analogous liquidus phase relations in the system $Na_2O–Al_2O_3–SiO_2$ (see also Osborn and Muan, 1960e). They related these changes in liquidus phase equilibria to a strong preference of Al^{3+} for three-dimensional network units in the melt. As a result, increasing Al/(Al + Si) is accompanied by greater relative abundance of TO_2 (T = Al + Si) units. In order to maintain mass-balance (constant NBO/T), the relative abundance of silicate anionic units with their NBO/T greater than that of the melt bulk must also increase. These abundance changes in the melts are, then, reflected in the changes in liquidus phase equilibria as a function of Al/(Al + Si) of the system.

It is evident from the above discussion that in the ranges of Al/(Al + Si), NBO/T, $Fe^{3+}/\Sigma Fe$ and total iron content of natural magmatic liquids, major changes in the liquidus equilibria of iron-free minerals take place simply as a function of the oxidation state of iron. The transition from anorthite to gehlenite as a liquidus phase is the most extreme example (NBO/T contrast of 3 across the liquidus boundary). In a tholeiitic liquid, the NBO/T typically is in the range 0.6–0.8 and the Al/(Al + Si) is 0.2–0.3 (see Mysen et al., 1982a, for calculations). From the model system calculations (Fig. 11) one may suggest, therefore, that a highly oxidized basalt could have tridymite (or quartz) on the liquidus. Reduction of ferric iron would result in the appearance of a metasilicate phase (pyroxene) and complete reduction in the stabilization of an orthosilicate (olivine) liquidus phase. It is clear, therefore, that the relationship between redox equilibria and melt structure is of major importance to the understanding of the liquidus equilibria of magmatic systems.

Acknowledgments

Critical reviews by H. S. Yoder, Jr. and two anonymous reviewers are appreciated.

References

Amthauer, G., Annersten, H., and Hafner, S. S. (1977) The Mössbauer spectrum of ^{57}Fe in titanium-bearing andradites. Physics and Chemistry of Minerals, 1, 339–413.

Amthauer, G., Langer K. and Schliestedt, M. (1980) Thermally activated electron delocalization in deerite. Journal of Physics and Chemistry of Minerals, 6, 19–30.

Annersten, H. and Halenius, U. (1976) Ion distribution in pink muscovite: a discussion. American Mineralogist, 61, 1045–1050.

Annersten, H. and Olesch, M. (1978) Distribution of ferrous and ferric iron in clintonite and the Mössbauer characteristics of ferric iron in tetrahedral coordination. Canadian Mineralogist, 16, 199–204.

Annersten, H., Olesch, M. and Seifert, F. A. (1978) Ferric iron in orthopyroxene: a Mössbauer spectroscopic study. Lithos, 11, 301–310.

Bell, P. M. and Mao, H. K. (1974) Crystal-field spectra of Fe^{2+} and Fe^{3+} in synthetic basalt glass as a function of oxygen fugacity. Carnegie Institution of Washington Year Book, 73, 496–497.

Brawer, S. A. (1975) Theory of the vibrational spectra of some network and molecular glasses. Physical Review B, 11, 3173–3194.

Brown, G. E., Keefer, K. D., and Fenn, P. M. (1978) Extended X-ray fine structure (EXAFS) study of iron-bearing silicate glass. (abstr.) Geological Society of America Abstracts with Programs, 10, 373.

Calas, G. and Petiau, J. (1983) Structure of oxide glasses: spectroscopic studies of local order and crystallochemistry: geochemical implications. Bulletin Mineralogique, 106, 33–55.

Calas, G., Levitz, P., Petiau, J., Bondot, P., and Loupias, G. (1980) Etude de l'order local autoudu fer dans les verres silicates naturels et synthetiques a l'aide de la spectrometrie d'absorption. X. Revue de Physique Appliquee, 15, 1161–1167.

Chou, I. M. (1978) Calibration of oxygen buffers at high P and T using the hydrogen fugacity sensor. American Mineralogist, 63, 690–703.

Coey, J. M. D., Moukarik, A. and McDonagh, C. M. (1982) Electron hopping in cronstedite. Solid State Communications, 41, 797–800.

Danckwerth, P. A. and Virgo, D. (1982) Structural state of Fe in the system Na_2O–SiO_2–Fe–O. Carnegie Institution of Washington Year Book, 81, 342–344.

Danckwerth, P. A., Virgo, D., and Mysen, B. O. (1982) The structural state of Fe in alkaline vs. alkaline-earth silicate systems. Carnegie Institution of Washington Year Book, 81, 344–347.

Davidon, W. C. (1959) Variable metric method for minimization. Argonne National Laboratory, ANL 5990.

Deines, P., Nafziger, R. H., Ulmer, G. C., and Woermann, E. (1974) Temperature–oxygen fugacity tables for selected gas mixtures in the system C–H–O at one atmosphere total pressure. Bulletin, Earth and Mineral Sciences, The Pennsylvania State University, 88.

Dickenson, M. P. and Hess, P. C. (1981) Redox equilibria and the structural role of iron in aluminosilicate melts. Contributions to Mineralogy and Petrology, 78, 352–358.

Domine, F. and Piriou, B. (1983) Study of sodium silicate melt and glass by infrared reflectance spectroscopy. Journal of Non-Crystalline Solids, 55, 125–131.

Douglas, E. W., North, P. and Paul, A. (1965) Oxygen ion activity on redox equilibrium in glasses. Physics and Chemistry of Glasses, 6, 216–223.

Evans, B. J. and Amthauer, G. (1980) The electronic structure of ilvaite and the pressure and temperature dependence of its ^{57}Fe Mössbauer spectrum. Journal of Physics and Chemistry of Solids, 41, 985–1001.

Fox, K. E., Furukawa, T., and White, W. B. (1982) Transition metal ions in silicate melts, Part 2, Iron in sodium silicate glasses. Physics and Chemistry of Glasses, 23, 169–178.

Furukawa, T., Fox, K. E., and White, W. B. (1981) Raman spectroscopic investigation of the structure of silicate glasses. III. Raman intensities and structural units in sodium silicate glasses. Journal of Chemical Physics, 75, 3226–3237.

Gaskell, P. H. (1975) Construction of a model for ordered amorphous tetrahedral materials using ordered units. Philosophical Magazine, 32, 211–229.

Goldman, D. S. (1983) Oxidation equilibrium of iron in borosilicate glass. Journal of the American Ceramic Society, 66, 205–209.

Hafner, S. S. and Huckenholz, H. G. (1971) Mössbauer spectrum of synthetic ferridiopside. Nature, Physical Science, 233, 255–261.

Haggerty, S. E. (1978) The redox state of planetary basalts. Geophysical Research Letters, 5, 443–446.

Haggerty, S. E. and Thompkins, L. A. (1983) Redox state of the earth's upper mantle from kimberlitic ilmenites. Nature, 303, 295–300.

Hart, S. E. and Davis, K. E. (1978) Nickel partitioning between olivine and silicate melt. Earth and Planetary Science Letters, 40, 203–220.

Hess, P. C. and Wood, M. I. (1982) Aluminum coordination in metaaluminous and peralkaline silicate melts. Contributions to Mineralogy and Petrology, 81, 103–112.

Holmquist, S. (1966) Ionic formulation of redox equilibria in glass melts. Journal of the American Ceramic Society, 49, 228–229.

Huggins, F. E., Mao, H. K. and Virgo, D. (1975) Mossbauer studies at high pressure. Carnegie Institution of Washington, Year Book 74, 405–410.

Irving, A. J. and Frey, F. A. (1978) Distribution of trace elements between garnet megacrysts and host volcanic liquids of kimberlitic to rhyolitic composition. Geochimica et Cosmochimica Acta, 42, 771–789.

Kilinc, A., Carmichael, I. S. E., Rivers, M. L., and Sack, R. O. (1983) The ferric–ferrous ratio of natural silicate liquids equilibrated in air. Contributions to Mineralogy and Petrology, 83, 136–141.

Kirkpatrick, R. J., Smith, K. A., Kinsey, R. A., and Oldfield, E. (1982) High-resolution ^{29}NMR of glasses and crystals in the system CaO–MgO–SiO_2. (abstr.) EOS, 63, 1140.

Larson, H. and Chipman, J. (1953) Oxygen activity in iron oxide slags, Transactions AIME, 196, 1089–1096.

Levitz, P., Bonnin, D., Calas, G., and Legrand, A. P. (1980) A two-parameter distribution analysis of Mössbauer spectra in non-crystalline solids using general inversion method. Journal of Physics E, Scientific Instruments, 13, 427–437.

Liebau, F. (1981) The influence of cation properties on the conformation of silicate and phosphate anions. In M. O'Keeffe and A. Navrotsky, Eds., Structure and Bonding in Crystals, Vol. 2, p. 197–232. Academic Press, New York.

Mao, H. K., Virgo, D., and Bell, P. M. (1973) Analytical study of the orange soil returned by the Apollo 17 astronauts. Carnegie Institution of Washington Year Book, 72, 631–638.

Mo, X.-X., Carmichael, I. S. E., Rivers, M., and Stebbins, J. (1982) The partial molar volume of Fe_2O_3 in multicomponent silicate liquids and the pressure dependence of oxygen fugacity in magmas. Mineralogical Magazine, 45, 237–245.

Mysen, B. O. and Virgo, D. (1978) Influence of pressure, temperature and bulk composition on melt structures in the system

$NaAlSi_2O_6$–$NaFe^{3+}Si_2O_6$. American Journal of Science, 278, 1307–1322.

Mysen, B. O. and Virgo, D. (1980) Trace element partitioning and melt structure: an experimental study at 1 atm pressure. Geochimica et Cosmochimica Acta, 44, 1917–1930.

Mysen, B. O. and Virgo, D. (1984a) Redox equilibria, structure and melt properties in the system Na_2O–Al_2O_3–SiO_2–Fe–O. Carnegie Institution of Washington Year Book, 82, 313–317.

Mysen, B. O. and Virgo, D. (1983b) Iron-bearing alkaline earth silicate melts: relations between redox equilibria of iron, melt structure and liquidus phase equilibria. Carnegie Institution of Washington Year Book, 82, 317–321.

Mysen, B. O. and Virgo, D. (1983c) Effect of pressure on the structure of iron-bearing silicate melts. Carnegie Institution of Washington, Year Book, 82, 321–325.

Mysen, B. O., Seifert, F. A. and Virgo, D. (1980a) Structure and redox equilibria of iron-bearing silicate melts. American Mineralogist, 65, 867–884.

Mysen, B. O., Virgo, D., and Scarfe, C. M. (1980b) Relations between the anionic structure and viscosity of silicate melts—a Raman spectroscopic study. American Mineralogist, 65, 690–711.

Mysen, B. O., Virgo, D., and Kushiro, I. (1981) The structural role of aluminum in silicate melts—a Raman spectroscopic study at 1 atm. American Mineralogist, 66, 678–701.

Mysen, B. O., Virgo, D., and Seifert, F. A. (1982a) The structure of silicate melts: implications for chemical and physical properties of natural magma. Reviews of Geophysics and Space Physics, 20, 353–383.

Mysen, B. O., Virgo, D., and Seifert, F. A. (1982b) Distribution of aluminum between anionic units in depolymerized silicate melts as a function of pressure and temperature. Carnegie Institution of Washington Year Book, 81, 360–366.

Mysen, B. O., Virgo, D., and Seifert, F. A. (1984) Redox equilibria of iron in alkaline earth silicate melts: relationships between melt structure, oxygen fugacity, temperature and properties of iron-bearing silicate liquids. American Mineralogist, 69, 834–847.

Mysen, B. O., Virgo, D. and Seifert, F. A. (1985) Relationships between properties and structure of aluminosilicate melts. American Mineralogist, 70, 88–105.

Nolet, D. A. and Burns, R. G. (1979) Ilvaite: a study of temperature dependent delocalization by the Mössbauer effect. Physics and Chemistry of Minerals, 4, 221–234.

Nolet, D. A., Burns, R. G., Flamm, S. L., and Besancon, J. R. (1979) Spectra of Fe–Ti silicate glasses: implications to remote-sensing of planetary surfaces. Proceedings, 10th Lunar Science Conference, 1775–1786.

O'Horo, M. P. and Levy, R. A. (1978) Effect of melt atmosphere on the magnetic properties of a $[(SiO_2)_{45}(CaO)_{55}]_{65}[Fe_2O_3]_{35}$ glass. Journal of Applied Physics, 49, 1635–1637.

Osborn, E. F. and Muan, A. (1960a) Phase equilibrium diagrams of oxide systems. Plate 2. The system CaO–Al_2O_3–SiO_2. American Ceramic Society, Columbus, Ohio.

Osborn, E. F. and Muan, A. (1960b) Phase equilibrium diagrams of oxide systems. Plate 10. The system CaO–"Fe_2O_3"–SiO_2. American Ceramic Society, Columbus, Ohio.

Osborn, E. F. and Muan, A. (1960c) Phase equilibrium diagrams of oxide systems. Plate 7. The system CaO–"FeO"–SiO_2. American Ceramic Society, Columbus, Ohio.

Osborn, E. F. and Muan, A. (1960d) Phase diagrams of oxide systems. Plate 3. The system MgO–Al_2O_3–SiO_2. American Ceramic Society, Columbus, Ohio.

Osborn, E. F. and Muan, A. (1960e) Phase diagrams of oxide systems. Plate 4. The system Na_2O–Al_2O_3–SiO_2. American Ceramic Society, Columbus, Ohio.

Paul, A. and Douglas, R. W. (1965) Ferrous–ferric equilibrium in binary alkali silicate glasses. Physics and Chemistry of Glasses, 6, 207–211.

Ryerson, F. J. and Hess, P. C. (1980) The role of P_2O_5 in silicate melts. Geochimica et Cosmochimica Acta, 44, 611–625.

Sack, R. O., Carmichael, I. S. E., Rivers, M., and Ghiorso, M. S. (1980) Ferrous–ferric equilibria in natural silicate liquids at 1 bar. Contributions to Mineralogy and Petrology, 75, 369–377.

Sato, M. (1972) Electrochemical measurements and control of oxygen fugacities with solid electrolyte systems. In G. C. Ulmer, Ed., Research Techniques for High Pressure and High Temperature, p. 43–99. Springer Verlag, New York.

Sato, M. and Valenza, M. (1980) Oxygen fugacities of the layered series of the Skaergaard intrusion, East Greenland. American Journal of Science, 280A, 134–158.

Seifert, F. A., Virgo, D., and Mysen, B. O. (1979) Melt structure and redox equilibria in the system Na_2O–FeO–Fe_2O_3–Al_2O_3–SiO_2. Carnegie Institution of Washington Year Book, 78, 511–519.

Seifert, F. A., Mysen, B. O., and Virgo, D. (1982) Three-dimensional network melt structure in the systems SiO_2–$NaAlO_2$, SiO_2–$CaAl_2O_4$ and SiO_2–$MgAl_2O_4$. American Mineralogist, 67, 696–718.

Taylor, M. and Brown, G. E. (1979a) Structure of mineral glasses. I. The feldspar glasses $NaAlSi_3O_8$, $KAlSi_3O_8$, $CaAl_2Si_2O_8$. Geochimica et Cosmochimica Acta, 43, 61–77.

Taylor, M. and Brown, G. E. (1979b) Structure of mineral glasses. II. The SiO_2–$NaAlSiO_4$ join. Geochimica et Cosmochimica Acta, 43, 1467–1475.

Thornber, C. R., Roeder, P. L., and Foster, J. R. (1980) The effect of composition of the ferric–ferrous ratio in basaltic liquids at atmospheric pressure. Geochimica et Cosmochimica Acta, 44, 525–533.

Virgo, D. and Mysen, B. O. (1985) The structural state of iron in oxidized vs. reduced glasses at 1 atm: a ^{57}Fe Mössbauer study. Physics and Chemistry of Minerals, in press.

Virgo, D., Mysen, B. O., and Seifert, F. A. (1981) Relationship between oxidation state of iron and structure of silicate melts. Carnegie Institution of Washington Year Book, 80, 308–311.

Virgo, D., Mysen, B. O., and Danckwerth, P. A. (1982) Speciation of Fe^{3+} in 1-atm Na_2O–SiO_2–Fe–O melts. Carnegie Institution of Washington Year Book, 81, 349–353.

Virgo, D., Mysen, B. O., and Danckwerth, P. A. (1983) Redox equilibria and the anionic structure of $Na_2O \cdot xSiO_2$–Fe–O melts: effect of oxygen fugacity. Carnegie Institution of Washington Year Book, 82, 305–309.

Watson, E. B. (1976) Two-liquid partition coefficients: experimental data and geochmemical implications. Contributions to Mineralogy and Petrology, 56, 119–134.

Watson, E. B. (1977) Partitioning of manganese between forsterite and silicate liquid. Geochimica et Cosmochimica Acta, 41, 1363–1374.

Waychunas, G. A. and Rossman, G. R. (1983) Spectroscopic standard for tetrahedrally coordinated ferric iron: $\gamma LiAlO_2 : Fe^{3+}$. Physics and Chemistry of Minerals, 9, 212–215.

Wivel, C. and Morup, S. (1981) Improved computational procedure for evaluation of overlapping hyperfine parameter distributions in Mössbauer spectra. Journal of Physics E, Scientific Instruments, 14, 605–610.

Manuscript received, February 7, 1984;
accepted for publication, November 19, 1984.